International Journal of Technical Innovation in Modern Engineering & Science (IJTIMES)
Impact Factor: 3.45 (SJIF-2015), e-ISSN: 2455-2585
Volume 3, Issue 08, August-2017

A Multivariable Sliding Mode Control Energy Management Strategy For Standalone DC Micro Grids

G Sasank Rahul[1], Prof. P Sujatha[2]

[1]*EEE Department & JNTUA College OF Engineering,*
[2]*EEE Department & JNTUA College OF Engineering,*

Abstract— In this paper, a planned and multivariable energy administration system is suggested that utilizes a wind turbine and a photovoltaic array of an independent DC micro grid as controllable generators by changing the pitch angle and the exchanging obligation cycles. The proposed technique is created as an sliding mode control (SMC) model predictive control. Applying to an example independent dc micro grid, the created controller understands the IU administration for charging the battery bank. The variable load requests are likewise shared precisely between generators in extent to their evaluations. In addition, the DC bus voltage is managed as a plan parameter.

Keywords—DC Microgrid, Sliding Mode Control(SMC), Energy Management strategy

I. INTRODUCTION

The near future distribution systems will comprise of a few interconnected micro grids that will locally produce, expend, and store energy [2]. A micro grid may work as an enlargement of the primary system, i.e., grid connected, or as an independent coordinate with no association with the grid. Independent dc micro grids have some unmistakable applications in flight, car, or on the other hand marine enterprises and in addition remote rustic zones. While ac systems experience the ill effects of the need of synchronization of a few generators [3-4], dc micro grids are more effective due to the truth that dc generators and storages needn't bother with ac dc converters for being connected with dc micro grids [2-5]. The three surely understood issues with respect to voltage control, control sharing, battery administration, are more serious in independent green micro grids, which comprise of just discontinuous solar and wind energy sources, and prompt the need of more refined control systems.

The security of a dc micro grid is measured as far as the security of its dc bus voltage level [6], which is one of the primary control destinations. The grid voltage source converters (G-VSCs) are the essential slack terminals to manage the voltage level of lattice connected micro grids .Battery banks, then again, are powerful slack terminals for independent micro grids; though their energy retaining limits are restricted with respect to various operational imperatives, as clarified later in this segment. Keeping in mind the end goal to direct the voltage level of independent dc micro grids, it has been shown the load shedding technique for the case in which there is lacking power generation or energy storage. Then again, introduce systems that reduce the inexhaustible power eras of independent dc micro grids if the battery bank can't assimilate the abundance generation. These reduction methodologies limit the batteries charging rate by the maximum retaining power; be that as it may, the greatest charging current should likewise be restricted. Besides, they don't shorten the energy of every generator in extent to its rating.

Keeping in mind the end goal to counteract over-focusing on conditions and circling streams between generators load requests should be shared between every single slack DG in extent to their evaluations. The traditional hang control strategy for dc slack terminals by supplanting the traditional curves with either a dc control dc voltage or a dc voltage-output current curve. In any case, independent dc micro grids are normally situated in little scale territories where the power sharing between DGs can be overseen by incorporated calculations which are less influenced by two issues: 1) Batteries in charging mode are nonlinear loads making curves the network voltage; and 2) The total voltage level of an independent micro grid is moved as the outcome of the load request variety.

Various marvels influence the batteries operation during the charging mode: 1) applying high charging currents, the batteries voltages rapidly reach to the gassing angle; 2) the inside resistor and thus control losses and warm impacts increment at high SOC levels; and 3) batteries can't be completely accused of a consistent high charging current. The work in limits, as an operational requirement, the maximum assimilated control by the batteries keeping in mind the end goal to shield them from failure. Notwithstanding, since batteries go about as nonlinear loads during the charging mode, it doesn't really confine the charging currents. Alternatively, the works in restricts the maximum attainable SOC that leads to unused capacities.

Contingent upon the extent of the power era to the load request proportion inside independent DC micro grids, three cases are visualized: 1) control generation and load request are adjusted; 2) load request surpasses control era causes dc bus voltage to drop without any load shedding; and 3) control generation is higher than load request drives batteries to be

cheated furthermore, bus voltage to climb. This examination concentrates on case (3) in which the produced control must be reduced on the off chance that it damages the batteries charging rates or if batteries are completely charged. A novel energy administration technique (EMS) is proposed to address, as its control destinations, three previously mentioned issues relating independent dc micro grids; i.e., dc bus voltage direction, relative power sharing, and battery administration.

Rather than the systems available in writing in which inexhaustible energy systems (RESs) dependably work in their MPPT mode, the proposed multivariable system utilizes a wind turbine what's more, a PV cluster as controllable generators and shortens their generations in the event that it is essential. The proposed EMS is created as an sliding mode control (SMC) model predictive control that constantly explains an ideal control issue (OCP) and finds the ideal estimations of the pitch angle and three exchanging obligation cycles. It at the same time controls four factors of micro grids: 1) control coefficient of the wind turbine; 2) speed of the wind generator; 3) working voltage of the PV array; and 4) charging current of the battery bank. It is demonstrated that, there are two main advantages of sliding mode control. First is that the dynamic behaviour of the system that may be tailored by the particular choice of the sliding function. Secondly, the closed loop response becomes totally insensitive to some particular uncertainties. This principle extends to model parameter uncertainties, disturbance and nonlinearity that are bounded. From a practical point of view SMC allows for controlling nonlinear processes subject to external disturbances and heavy model uncertainties.

II. SYSTEM DESCRIPTIONS AND MODELING

The independent dc micro grid in Fig. 1 is a little scale micro grid for remote applications. The wind turbine works at variable speeds and is connected with the electrical generator specifically, i.e., the immediate drive coupling. The variable speed operation is more adaptable for the power administration and MPPT application. Besides, coordinate drive coupling is more productive furthermore, solid and is more mainstream for little scale wind turbines. In spite of high cost, permanent magnet synchronous generators (PMSGs) are of direct drive generators in the market, mainly because of higher proficiency. From Fig. 1, it can be seen that battery bank is connected to the dc bus through a dc-coupled structure, i.e., by means of a dc-dc converter, which is more adaptable as far as actualizing extraordinary charging and releasing administrations regardless of more power losses.

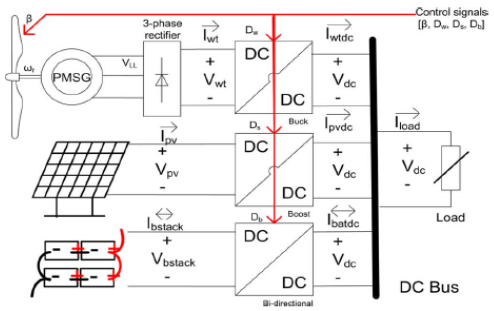

Fig. 1 Topology of a small-scale and standalone dc micro grid

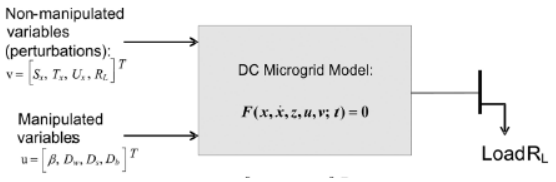

$$x = \lfloor I_f, Q_{act}, \omega_r \rfloor$$

$$z = (I_{pv}, V_{pv}, I_{pvdc}, I_{batdc}, V_{batack}, I_{wt}, V_{wt}, I_{wtdc}, T_g, T_m, \lambda, C_p, SOC, I_{load}, V_{dc})^T$$

Fig.2 Modified version of the system.

The developer displayed a scientific model of independent green dc micro grids as crossover differential mathematical conditions. condenses an altered adaptation of the proposed display. Since this paper concentrates on the case in which there is an over abundance control more noteworthy than or measure up to the maximum conceivable retaining rate of the battery bank, the crossover nature of the battery bank operation is overlooked for the purpose of straight forwardness. The differential and logarithmic states, i.e., what's more, and the controlled and non-controlled control factors, to be specific, and, are point by point later all through the following sub-segments. In what takes after, the accompanying documentations are utilized to show the independent dc micro grid in Fig. 1 as DAEs:

$$\mathcal{F}(x,\dot{x},z,u,v)=\begin{bmatrix} f_1(x,\dot{x},z,u,v) \\ f_2(x,\dot{x},z,u,v) \\ \ddot{f}_{24}(x,\dot{x},z,u,v) \end{bmatrix}=0 \qquad (1)$$

Where $\mathcal{F}$ is a set of implicit differential and algebraic functional for $i \in \{1,2,...,24\}$. The first two constraints f_1 and f_2 are due to the fact that in standalone dc micro grids the sum of the generated, stored, and consumed powers is always zero.

$$f_1 = V_{dc}(I_{pvdc} + I_{\omega tdc} + I_{batdc} + I_{load}) \quad (2a)$$

$$f_2 = V_{dc} - I_{load} R_L \qquad (2b)$$

A. Wind Branch

Execution of the wind turbines is measured as the power coefficient curve as for the tip speed proportion and pitch angle. Condition (3) demonstrates the power coefficient bend of three-sharp angle wind turbines.

$$f_3 = C_{p,nom} - \frac{1}{C_{p,max}} \times C_1 \left(\frac{C_2}{\lambda_i} - C_3\beta - C_4\right) \exp\left(-\frac{C_5}{\lambda_i}\right) + C_6\lambda \qquad (3a)$$

$$f_4 = \lambda - \frac{Rad \times \omega_r}{U_x} \qquad (3b)$$

$$f_5 = \lambda_i - \left(\frac{1}{\lambda + 0.08\beta} - \frac{0.035}{\beta^3 + 1}\right)^{-1} \qquad (3c)$$

Where λ and β_w separately, are the tip speed proportions and pitch point. R_{ad} is the span of the angles and $C_{p,max}$ is the greatest achievable power coefficient at the ideal tip speed proportion of λ_{opt}. The trial coefficients are characterized is a middle of the road variable. Condition (4) shows the connected PMSG generator.

$$f_6 = \frac{d\omega_r}{dt}(t) - \frac{1}{J}(T_e - T_m - F\omega_r), \qquad (4a)$$

$$f_7 = -T_e \times \omega_r - I_{wtdc} \times V_{dc}, \qquad (4b)$$

$$f_8 = -T_m \times \omega_r - \left(C_{p,norm}\left(\frac{U_x}{Ux,base}\right)^3 P_{nom}, \qquad (4c)$$

Energy administration methodologies of micro grids must gauge the dc bus voltage level deviation from its set point in about each 5–10s. It implies that aside from the speed of the generator (4a) all other quick voltage and current flow can be overlooked. It is additionally accepted that there is no mechanical what's more, electrical losses through the power train and in this way the electromagnetic power given by (4b) is equivalent to the output electrical energy of the wind branch. Condition (4c) demonstrates that the PMSG is connected straightforwardly to turbine, which turns at low speed, and in this way needs different shaft sets. Henceforth, the electrical recurrence is P times speedier than the mechanical precise speed. The pole inactivity J(Kg.m^2) and the joined thick grating coefficient F(N.m.s) of PMSG are given by the producers.

For energy administration techniques, the normal model of the buck converter is supplanted with the enduring state conditions for the persistent conduction mode (CCM).

$$f_9 = V_{dc} - D_w V_{wt}, \qquad (5a)$$

$$f_{10} = I_{wt} - D_w I_{wtdc} \qquad (5b)$$

Where D_w is the switching duty cycle of the converter and all remaining parameters are as depicted in Fig. 1.
The average dc output voltage of the rectifier, $V_{wt,}$ in presence of the non-instantaneous current commutation is calculated as follows:

$$V_{\omega t} = 1.35V_{LL} - \frac{3}{\Pi} W_e L_s I_{\omega t} \qquad (6)$$

Eq (6) having that the number of the pole pairs and the flux linkage $\varphi(V.s)$ and replacing V_{LL}, i.e., the r.m.s. value of the line-to-line output voltage of the generator, with, $\sqrt{3}/_2 P\varphi\omega_r$ one calculates the dc output current of the wind branch, as follows:

$$f_{11} = I_{wtdc} - \frac{\pi}{3P\omega_r L_s D_W}\left\{\frac{1.35\sqrt{3}P\psi\omega_r}{\sqrt{2}} - \frac{V_{dc}}{D_W}\right\} \quad (7)$$

B. Battery Branch

The charging operation of a lead acid battery bank, consisting of N_{batp} X N_{bats} batteries, is modeled as (8):

$$f_{12} = \frac{V_{bstack}}{N_{bats}} - V_o + R_{bat}\frac{I_{bstack}}{N_{batp}} + \frac{P_1 C_{max}}{C_{max} - Q_{act}}Q_{act} + \frac{P_1 C_{max}}{Q_{act} + 0.1C_{max}}I_f, (8a)$$

$$f_{13} = \frac{dQ_{act}}{dt}(t) - \frac{1}{3600}\frac{I_{bstack}(t)}{N_{batp}}, \quad (8b)$$

$$f_{14} = \frac{dI_f}{dt}(t) + \frac{1}{T_n}\left(I_f - \frac{I_{bstack}}{N_{batp}}\right), \quad (8c)$$

$$f_{15} = V_{bstack} - \frac{V_{dc}}{1 - D_b}, \quad (8d)$$

$$f_{16} = I_{bstack} - (1 - D_b)I_{batdc}, \quad (8e)$$

$$f_{17} = SOC - \left\{1 - \frac{Q_{act}}{C_{max}}\right\} \quad (8f)$$

where V_{bstack}, I_{bstack}, and SOC are, respectively, the voltage, current, and state of charge of the battery bank. I_f is the filtered value of the battery current with the time constant of T_s and Q_{act} is the actual battery capacity. The experimental parameter P_1 requires being identified for each type of battery while the maximum amount of the battery capacity, C_{max}, internal resistor of battery, R_{bat} and the battery constant voltage, V_o, are given by manufacturers. By ignoring the discharging mode of the battery bank operation, the bi-directional converter acts as a boost type converter.

C. Solar Branch

The equivalent electrical circuit of the PV module is used to mathematically model the solar branch, consisting of a PV array and a boost converter. Eq. (9) shows the characteristic equations of a PV array, consisting of V_{pvp} X N_{pvs} PV modules:

$$f_{18} = I_{pv} - I_{ph} + I_o\left\{\exp\left(\frac{V_{pv} + \frac{N_{pvn}}{N_{pvp}}R_s I_{pv}}{n_d N_s}\frac{q \times N_{pvs}}{KT_c}\right) - 1\right\} + \frac{V_{pv} + \frac{N_{pvs}}{N_{pvp}}R_s I_{pv}}{\frac{N_{pvs}}{N_{pvp}}R_{sh}}, \quad (9a)$$

$$f_{19} = I_{ph} - N_{pvp}\times\left(\frac{R_s + R_{sh}}{R_{sh}}I_{sc,stc} + k_1(T_c - T_{c,stc})\right)\frac{S}{S_{stc}}, \quad (9b)$$

$$f_{20} = I_o - N_{pvp}\times\frac{I_{sc,stc} + k_1(T_c - T_{c,stc})}{\exp\left(\frac{V_{oc,stc} + k_v(T_c - T_{c,stc})}{n_d N_s}\frac{q}{KT_c}\right) - 1} \quad (9c)$$

Where I_{ph} denotes the photocurrent and I_o is the diode reverse saturation current. R_s and R_{sh}, respectively, are the series and parallel equivalent resistors of each PV module and all other parameters are as follows:

Similar to the wind branch, the average model of the boost converter is replaced with the steady-state equations for CCM :

$$f_{21} = V_{pv} - (1 - D_s)V_{dc}, \qquad (10a)$$

$$f_{22} = I_{pvdc} - (1 - D_s)I_{pv}. \qquad (10b)$$

III. CONTROLLER DESIGN

A. Optimal Control Problems (OCPs) and Nonlinear Model Predictive Control (NMPC)

OCPs, as shown in equation (11), make unequivocal utilization of the system show, given by (11b), keeping in mind the end goal to locate an ideal control law $\mu^*(.)$, which meets number of correspondence and disparity imperatives. The term ideal here is characterized as for a specific measure that infers the control targets. This basis is determined with a cost practical J, comprising of the Lagrangian expression $\mathcal{L}$ and the terminal cost term $\mathcal{M}$. While the Lagrangian expression demonstrates the cost work during the time frame, the terminal cost punishes last esteems. Conditions (11d) and (11e), individually, figure the last and starting imperatives which must be kept up by the ideal arrangement. In addition, (11g) speaks to boxing limitations on the states and control factors:

$$u^*(.) = \underset{u(.) \in \mathfrak{R}^n}{\arg minimize}\ J(x(t), z(t), u(t), T)$$

$$:= \int_t^{t+T} \mathcal{L}\big(x(\tau), z(\tau), u(\tau)\big)d\tau + \mathcal{M}\big(x(T), z(T)\big) \qquad (11a)$$

$$s.t.: \mathcal{F}\big(x(t), \dot{x}(\tau), z(\tau), u(\tau), v(\tau)\big) = 0 \qquad (11b)$$

$$\mathcal{H}\big(x(\tau), z(\tau), u(\tau)\big) \leq 0 \qquad (11c)$$

$$\mathcal{R}\big(x(T), z(T)\big) = 0 \qquad (11d)$$

$$x(\tau) = x_0, z(\tau) = z_0 \qquad (11e)$$

$$\forall \tau \epsilon [t, t+T] \qquad (11f)$$

$$x(\tau)\epsilon\chi, z(\tau)\epsilon\mathcal{Z}, u(\tau)\epsilon\mathcal{U}. \qquad (11g)$$

OCPs are open-circle systems and are wrapped by a criticism circle to build NMPC techniques. NMPC systems, which are additionally called as the retreating skyline control, persistently comprehend an OCP over a limited skyline utilizing the estimations acquired at as the underlying esteems. At that point the first ideal esteem is connected as the following control flag. Looking at with the traditional strategies, NMPCs are intrinsically nonlinear what's more, multivariable techniques that handle requirements and delays.

There are three unique procedures to discretize and illuminate OCPs of (11): 1) dynamic programming strategy in view of the Bellman's optimality standard; 2) circuitous technique based on the Pontryagin least standard; and 3) coordinate techniques that change over OCPs into nonlinear improvement issues (NLPs) which are then fathomed by NLP solvers. In this paper, a direct strategy, named collocation discretization, is created in CasADi condition. CasADi actualizes the programmed separation (AD) method to diminish the controller execution time. It utilizes the notable inside point streamlining agent (IPOPT) instrument to tackle the subsequent NLPs.

B. Control System

Fig. 3 represents the dc micro grid and the proposed ideal EMS. Since it concentrates on the charging method of the battery operation, just the left side of the connected bi-directional converter is appeared. The proposed EMS progressively gets the evaluated system states, $\hat{x}$, as sources of info and figures the ideal arrangement, $\mu^*(.)$ as outputs. The outside state estimator and the indicator of the non-controlled factors are out of the extension of this paper. venture ahead expectations of the sunlight based irradiance, wind speeds, and load requests are removed either from a meteorological focus or an outer indicator utilizing autoregressive- moving-normal (ARMA) system. The bus voltage level of the micro grid, V_{dc}, is set remotely and subsequently the created controller can go about as the auxiliary and essential levels of the progressive engineering.

`

The created NMPC controller comprises of three substances: 1) the dynamic analyzer that progressively understands OCP at each inspecting time h, 2) the scientific model, $\mathcal{F}$, of the system to anticipate its conduct; and 3) the

cost work furthermore, requirements of the pertinent OCP. The ideal pitch point $\overline{\beta}$, is connected as a set point to an inward shut circle controller. Additionally, the ideal estimations of the exchanging obligation cycles are connected to the beat width modulators (PWMs) of the dc-dc converters. the plan parameters and computational times of the created NMPC controller. The computational times are computed on an Intel CORE 2 DOU machine with 3 GB of RAM. The exhibited times in show that the micro grid voltage level deviation from the set point is assessed each 5 s that consents to the progressive design details.

C. Sliding Mode Control:

The control algorithm using sliding Mode controller is used for maximum power extraction from PV Array at various operating conditions. This control strategy provides accurate estimation of point corresponding to maximum power on PV curve and helps to increase its efficiency. The designing of SMC includes two main steps as designing a switching function called sliding surface and a control law.

$$u = \begin{cases} \Rightarrow 1; \ if \ i_{fs} > 0 \\ \Rightarrow 0; \ if i_{fs} < 0 \end{cases}$$

1) Control Objectives*:*

Three aforementioned control objectives, i.e., dc bus voltage regulation, proportional power sharing, and implementing the IU regime to charge batteries, are formulated by two slack variables in (12) and (13) and the cost function in (14):

$$f_{23} = \alpha_1 - (V_{dc} - \overline{V}_{dc}) \qquad (12)$$

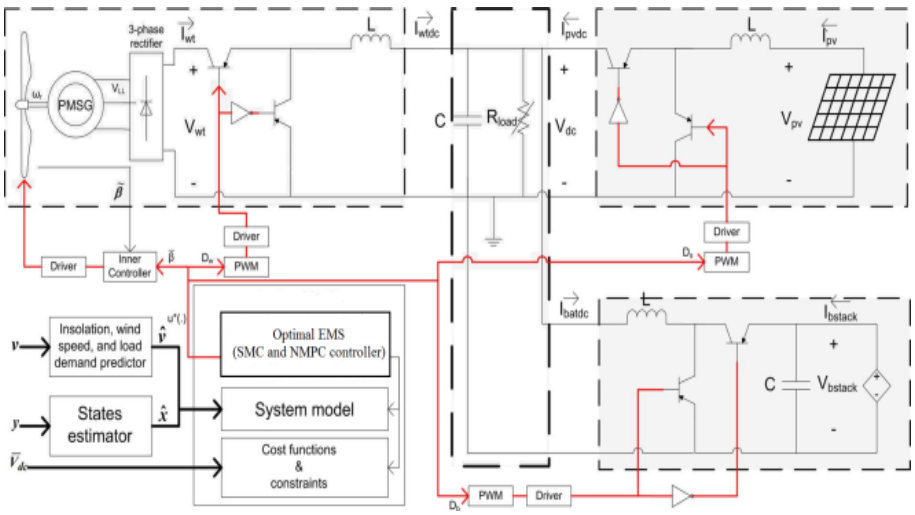

Fig. 3. Simplified view of the dc micro grid with the developed NMPC and sliding mode controller. The battery bank is assumed to work in charging mode,

The permissible deviation of the dc bus voltage level V_{dc} from the specified set point $\overline{V_{dc}}$ is defined by a slack variable $\alpha_1$in (12). It is a design parameter set to $\pm 0.02\,\overline{V_{dc}}$ or equivalently ± 0.96 volt for a 48.0-volt dc bus:

$$f_{24} = \propto_2 - \left\{ \frac{I_{wtdc} V_{dc}}{P_{wt,nom}} \left(\frac{U_{x,base}}{\max(U_x, U_{x,base})} \right)^3 - \frac{I_{pvdc} V_{dc}}{P_{pv,nom}} \frac{S_{x,base}}{\max(S_x, S_{x,base})} \right\}. \qquad (13)$$

The permissible deviation from the proportional power sharing criterion is given in (13) as a slack variable α_2 the design parameter is set to $\pm 1\%$ increase the flexibility of the algorithm with the cost of a slight penalty. The generated powers are normalized with respect to the wind speed and insolation values, i.e.,U_x and S_{xm}

The IU charging regime is modeled as two cost functions for two separate cases:

$$J(x(n),z(n),u(n),N) := \sum_{k=n}^{n+N} \left\{ \beta_1 \| \frac{1}{\bar{I}_c} \left(\frac{I_{bstack}(k)}{N_{batp}} - \bar{I}_c \right) \|_2 + \beta_2 \| \frac{V_{dc}(k) - \bar{V}_{dc}}{\bar{V}_{dc}} \|_2 \right\} + \left\{ \beta_1 \| \frac{1}{\bar{I}_c} \left(\frac{I_{bstack}(N)}{N_{batp}} - \bar{I}_c \right) \|_2 + \beta_2 \| \frac{V_{dc}(N) - \bar{V}_{dc}}{\bar{V}_{dc}} \|_2 \right\}, \quad (14a)$$

$$J(x(n),z(n),u(n),N) := \sum_{k=n}^{n+N} \left\{ \beta_3 \| \left(\frac{V_{bstack}(k) - N_{bats}V_{gas}}{N_{bats}V_{gas}} \right) \|_2 + \beta_4 \| \frac{V_{dc}(k) - \bar{V}_{dc}}{\bar{V}_{dc}} \|_2 \right\} + \left\{ \beta_3 \| \left(\frac{V_{bstack}(k) - N_{bats}V_{gas}}{N_{bats}V_{gas}} \right) \|_2 + \beta_4 \| \frac{V_{dc}(N) - \bar{V}_{dc}}{\bar{V}_{dc}} \|_2 \right\}, \quad (14b)$$

when the battery voltage level is not as much as the gassing voltage, the proposed controller utilizes (14a) to accuse the battery bank of the consistent current $\overline{I_c}$. Once the battery voltage level surpasses the gassing voltage the controller changes to (14b) to keep up it beneath the gassing voltage V_{gas} and shield batteries from permanent failure. Keeping in mind the end goal to keep the dc bus voltage level from staying at the upper or lower limits, the cost capacities are characterized as raised mixes of destinations with the weights β_1 - β_4. While β_1 and β_3 are near close to 1.0, β_2 and β_4 are near zero.

2) Box Constraints: Equation (15) includes the pitch angle control highlight to the created EMS keeping in mind the end goal to restrict the delivered streamlined power by the wind turbine:

$$0 \leq -T_e \omega_r \leq P_{wt,nom}. \quad (15)$$

The other box constraints on the manipulated variables and the system states are formulated as follows:

$$x_{min} \leq x \leq x_{max}, \quad (16a)$$

$$u_{min} \leq u \leq u_{max}, \quad (16b)$$

For instance, the duty cycles are limited between 20% and 80% and the pitch angle should be less than 30 degrees. 3) Initial Constraints: Prior to calculating the optimal solution over the next receding horizon N, all system states, i.e., $[\omega_r, Q_{act}, I_f]^T$ as well as the dc bus voltage level are initialized by the measured or estimated values.

IV. RESULTS

Results for the proposed system are executed. The results of the system are mentioned in the graphs as shown in the figures 4.1 - 4.16.

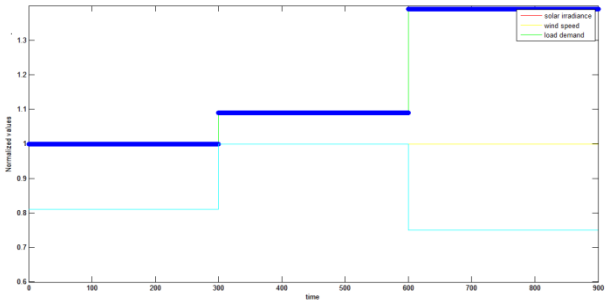

Fig. 4.1 Normalized amounts of non manipulated inputs

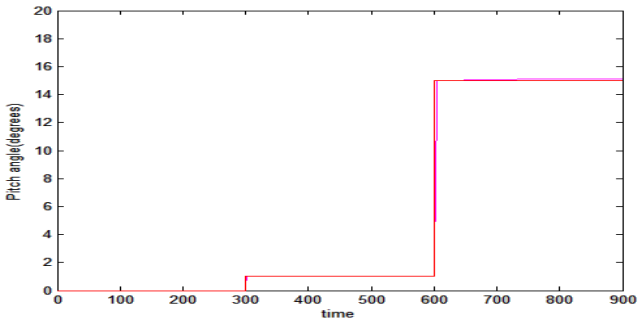

Fig.4.2. Pitch angle and switching duty cycles

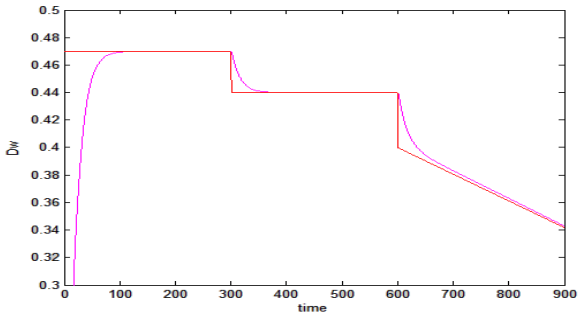

Fig.4.3. Wind branch converters

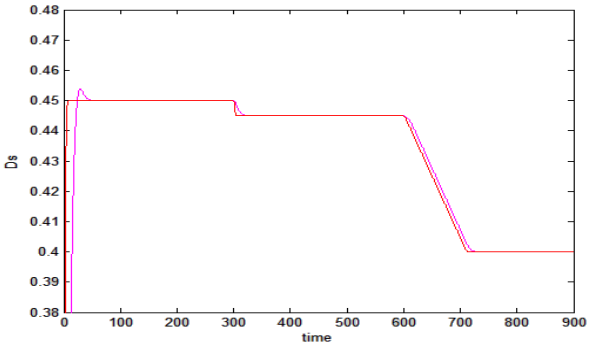

Fig.4.4. Solar branch converters

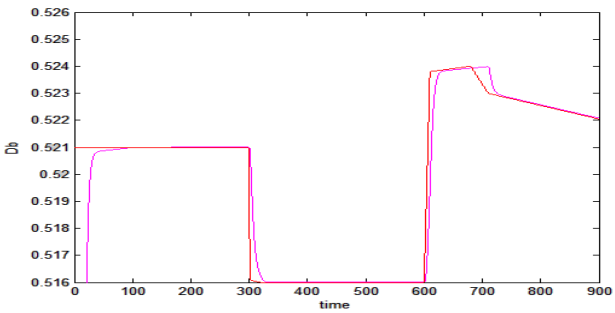

Fig.4.5. Battery branch converters

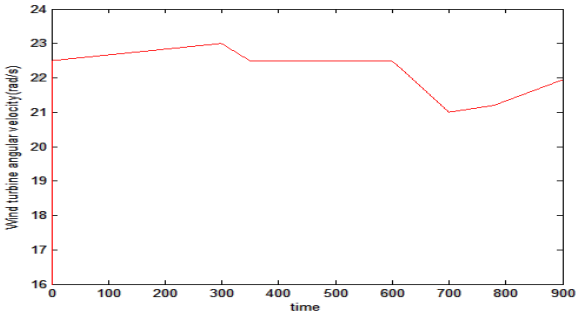

Fig.4.6.Angular velocity of wind turbine

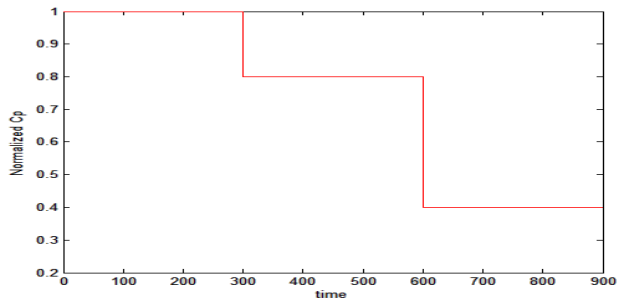

Fig.4.7. Power coefficient of PV array

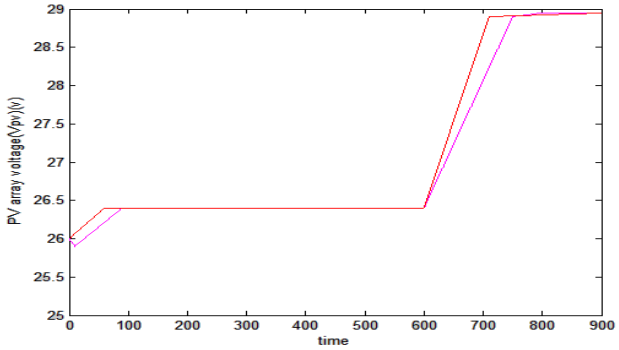

Fig. 4.8.Voltage of PV array

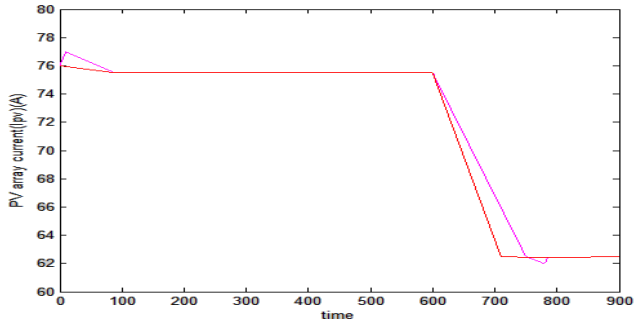

Fig. 4.9.Current of PV array

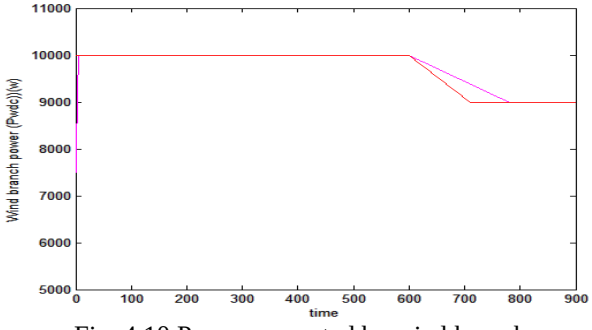

Fig. 4.10.Power generated by wind branch

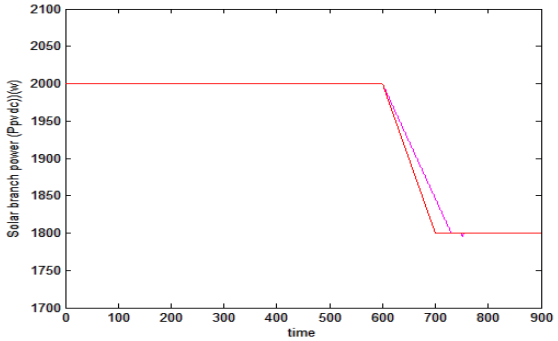

Fig. 4.11.Power generated by solar branch

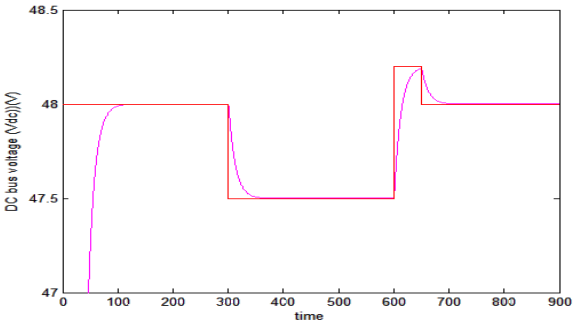

Fig. 4.12. The dc bus voltage of the micro grid

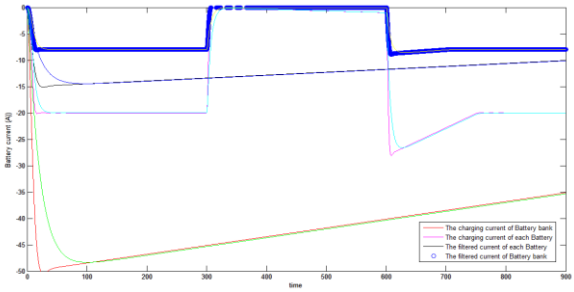

Fig. 4.13 Battery Charging current

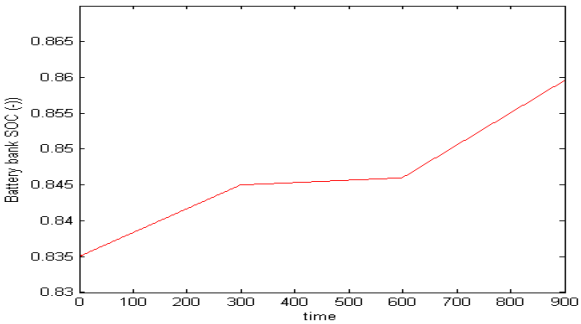

Fig. 4.14. SOC of the battery bank

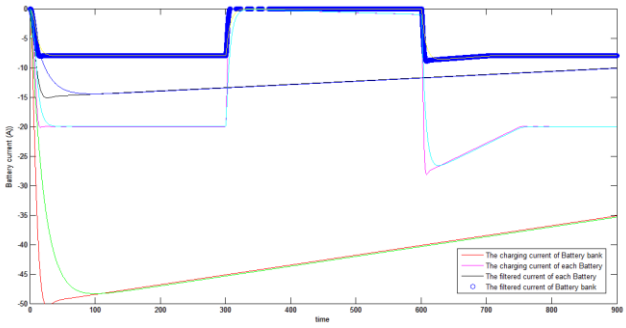

Fig. 4.15. Battery Charging current

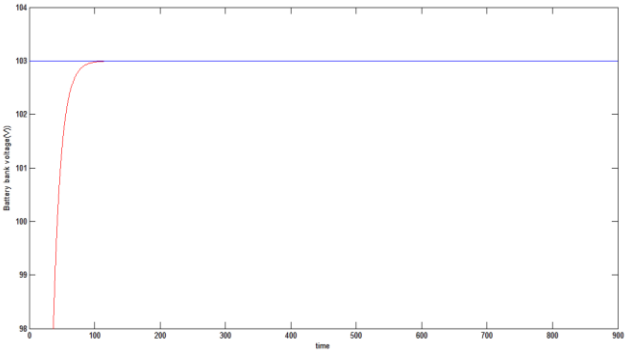

Fig. 4.16 Battery terminal voltage

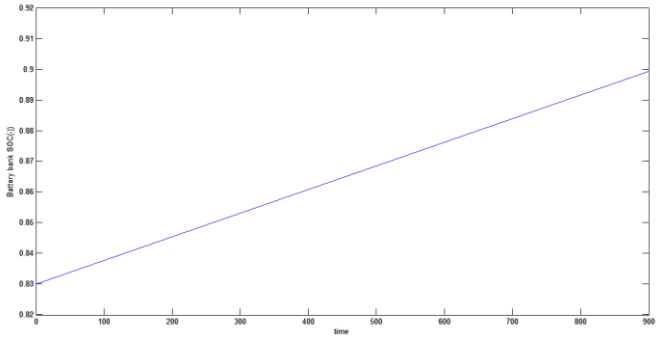

Fig. 4.17 SOC of the battery bank

A. Scenario I: Constant Current Charging Mode

Fig. 4.1 illustrates the normalized wind speed, insolation, and load demand inputs to the system. Wind speed starts at the rating value of the generator and sharply increases by 37.5% at t=600s. Load demand is below the nominal value, except between 300 to 600s. More over, solar irradiance is constant during the simulation only for results clarification for both controlling techniques.

The wind branch operates at MPPT mode up to t=300 seconds with a calculated pitch angle of zero as given in Fig. 4.2 Fig. 4.3 shows the calculated buck converter duty cycle that adjusts the rotational speed of the wind turbine at its nominal value, as given by Fig. 4.6. Fig. 4.7 indicates that the resulting power coefficient reaches to its maximum value.
At t = 300 and 600 s, the pitch angle goes up to 1.2 and 16 degrees, respectively, to promote the pitching to feather.

Fig. 4.6 and 4.7 illustrates a combination of the speed and power coefficient variations that curtails the generation down to 9.039 KW after t=600s, as given by Fig. 4.10 describes the gradual increase in the power generated by the wind branch in the proposed system.

Fig. 4.8 and 4.9 illustrates that though the PV array initially operates at its MPP, i.e., $V_{pv} = 26.3v$ and $I_{pv} = 76.1A$ after t=600s. In the proposed system constant variation in the voltage and current of the system is executed.

In spite of significant wind speed and load demand variations, Fig. 4.12 depicts that the dc bus voltage level stays within the permissible range, i.e., $48.0 \pm 0.96V$. Direct constant voltage is obtain from the initial time in the proposed system.

B. Scenario II: Constant Voltage Charging Mode

Once the battery terminal voltage reaches the gassing voltage, the charging current should be gradually reduced in order to maintain the voltage below the gassing level and fully charge the battery without the risk of permanent damage can be overcame in the proposed method also.
For the same wind speed and insolation variations as Scenario I, Fig. 4.15 and 4.16 respectively, show the charging current and terminal voltage variations of the battery bank. From Fig. 4.15 it can be seen that the battery bank is charged with a constant current equals to $0.31C_{10}$ up to t=300 s. Then, the controller starts gradually reducing the charging current in order to maintain the battery bank voltage constant.

V. CONCLUSION

In this paper, a novel ideal EMS that oversees the energy streams over an independent green dc micro grid, comprising of the wind, sun based, and battery branches. Sliding mode control (SMC) is a nonlinear control technique featuring remarkable properties of accuracy, robustness, and easy tuning and implementation of three primary control targets of independent dc micro grids. These goals are the voltage level control, relative power sharing, and battery administration. With a specific end goal to address these destinations, the created EMS at the same time controls the pitch angle of the wind turbine and the exchanging obligation cycles of three dc-dc converters. It has been demonstrated that the created controller tracks the MPPs of the wind and solar branches inside the ordinary conditions furthermore, reduces their generations during the under load conditions. The gave adaptable generation decrease system understands the steady current-consistent voltage charging administration that possibly expands the life expectancy of the battery bank. It is critical to take note of that the proposed procedure can be utilized as a unified execution of the essential and auxiliary levels in the various levelled design.

VI. FUTURE SCOPE

Future work will address the problem of reducing controller complexity and evaluating its robustness against parameter uncertainty the problem of precise tracking of desired trajectory in presence of unknown sea currents also warrants further consideration.

This work can be expanded by applying adaptive fractional FSMC, robust fuzzy terminal SMC and an adaptive fuzzy quasi continuous high order SMC for regulating for various parameters in Energy management strategy

REFERENCES

[1] Arash M. Dizqah, Alireza Maheri, Krishna Busawon, and Azadeh Kamjoo "A Multivariable Optimal Energy Management Strategy for Standalone DC Micro grids" IEEE transactions on power systems, VOL. 30, NO. 5, september 2015

[2] J. M. Guerrero, M. Chandorkar, T. Lee, and P. C. Loh, "Advanced Control Architectures for Intelligent Microgrids-Part I: Decentralized and Hierarchical Control," IEEE Trans. Ind. Electron., vol. 60, no. 4, pp. 1254–1262, 2013.

[3] R. S. Balog, W. W. Weaver, and P. T. Krein, "The load as an energy asset in a distributed DC smartgrid architecture," IEEE Trans. Smart Grid, vol. 3, no. 1, pp. 253–260, 2012.

[4] J. M. Guerrero, P. C. Loh, T. L. Lee, and M. Chandorkar, "Advanced Control Architectures for Intelligent Micro grids-Part II: Power quality, energy storage, and AC/DC micro grids," IEEE Trans. Ind. Electron., vol. 60, no. 4, pp. 1263–1270, 2013.

[5] N. Eghtedarpour and E. Farjah, "Control strategy for distributed integration of photovoltaic and energy storage systems in DC micro-grids," Renew. Energy, vol. 45, no. 0, pp. 96–110, 2012.

[6] D. Chen and L. Xu, "Autonomous DC voltage control of a DC micro grid with multiple slack terminals," IEEE Trans. Power Syst., vol. 27, no. 4, pp. 1897–1905, Nov. 2012.